ASCE

One-Dimensional Nonlocal Model for Gyratory Compaction of Hot Asphalt Mixtures

Tianhao Yan, S.M.ASCE[1]; Mihai Marasteanu[2]; and Jia-Liang Le, M.ASCE[3]

Abstract: Gyratory compaction has widely been used to evaluate the compactability of hot asphalt mixtures. Existing efforts on modeling of gyratory compaction have largely been devoted to sophisticated high-fidelity numerical simulations. This paper presents a one-dimensional nonlocal model for gyratory compaction. The model is anchored by the principle of mass conversation, in which the local densification rate is formulated as a function of the nonlocal packing fraction. The nonlocal model involves a material characteristic length scale, which is independent of the specimen size. The nonlocality gives rise to strong effects of the specimen height on the overall compaction curve as well as on the profile of the local packing fraction. A set of gyratory compaction experiments is performed on specimens of different heights. It is shown that the model is able to capture the measured size effect on the compaction curves. A parametric study is carried out to investigate the effects of nonlocality and model parameters on the predictions of compaction curve and profile of packing fraction.
DOI: 10.1061/(ASCE)EM.1943-7889.0002073.

Introduction

Compaction of the asphalt mixture is an essential step of the construction of asphalt pavements. During the compaction, asphalt binder, aggregates, and fines are subjected to a combination of compressive and shear forces as well as external vibration. The compaction process directly determines the final air void ratio of the asphalt mixtures and therefore has significant consequences for the durability and resilience of asphalt pavements (Finn and Epps 1980; Hughes 1989; Linden et al. 1989; Vivar and Haddock 2006; Willoughby and Mahoney 2007; Yan et al. 2021a). A high air void ratio would lead to a low material strength (Li and Marasteanu 2010) and at the same time to an increased moisture susceptibility (Cooley et al. 2001). On the other hand, an overcompacted mixture would be sensitive to high temperature (Archilla and Madanat 2001). Therefore, understanding the compaction process is of critical importance for design of asphalt pavements.

Over the last decades, extensive efforts have been devoted to experimental investigations of compaction of asphalt mixtures in laboratory settings. Many different laboratory compaction testing methods, such as Marshall impact compaction, kneading compaction, and gyratory compaction, have been developed (Harman et al. 2002; Consuegra et al. 1989). Among these methods, gyratory compaction is considered one of the best approaches to simulate the field compaction process (Consuegra et al. 1989). It was adopted in the United States as the laboratory compaction method for asphalt mixture design (e.g., Superpave mixture design method) [AASHTO M 323 (AASHTO 2013)]. Experimental investigations of gyratory compaction led to the development of different compaction indices, such as compaction slope (Moutier 1974; Leiva and West 2008), locking point (Vavrik and Carpenter 1998; Leiva and West 2008), and energy indices (Stakston et al. 2002; Faheem et al. 2005). Based on these indices, different empirical correlations between material properties and compactability were established. For example, it was observed that mixtures with more angular aggregates or less binder content are more difficult to compact (Stakston et al. 2002; Dessouky et al. 2004; Leiva and West 2008).

With advances in computational tools, major research efforts have been directed toward numerical modeling of the compaction process of asphalt mixtures. The existing computational models can be divided into two categories, the continuum and discrete modeling approaches. The continuum approach relies on the material constitutive models. In some early attempts, the critical state model of soil mechanics was adopted for finite-element simulations of the compaction of asphalt mixtures (Ter Huerne et al. 2008). In recent studies (Koneru et al. 2008; Masad et al. 2014a, b; Karimi et al. 2019), finite-strain elastoviscoplasticity models were extended to modeling the compaction of asphalt mixtures. The continuum models have been successfully used to simulate both the gyratory compaction and field compaction of asphalt mixtures. These models are computationally efficient for large-scale simulations. However, due to the nature of continuum modeling, the models do not explicitly capture the effect of mesoscale features, such as aggregate shape and size distribution, on the compactability of asphalt mixtures.

In the discrete models, the asphalt mixture is modeled as an assembly of particles (aggregates), and a specific contact model is used to describe the particle interaction. The main advantage of the discrete approach is that it explicitly captures the shape and size distribution of aggregates, which are believed to have a significant influence on the compaction performance. Chen et al. (2013, 2014) used the discrete element method to simulate different laboratory compaction experiments including gyratory compaction, vibration, and kneading. In the simulation, a viscoelastic–plastic contact law was used to describe the aggregate interaction. In recent studies, more realistic shapes of aggregates (e.g., elongated and flat aggregates), obtained from X-ray scan, were considered in discrete modeling (Liu et al. 2017; Gong et al. 2018b, a; Liu et al. 2018). The model was used to investigate the shape effect of coarse aggregates

[1]Graduate Research Assistant, Dept. of Civil, Environmental, and Geo-Engineering, Univ. of Minnesota, Minneapolis, MN 55455. ORCID: https://orcid.org/0000-0003-0706-3189

[2]Professor, Dept. of Civil, Environmental, and Geo-Engineering, Univ. of Minnesota, Minneapolis, MN 55455.

[3]Professor, Dept. of Civil, Environmental, and Geo-Engineering, Univ. of Minnesota, Minneapolis, MN 55455 (corresponding author). ORCID: https://orcid.org/0000-0002-9494-666X. Email: jle@umn.edu

Note. This manuscript was submitted on May 7, 2021; approved on October 19, 2021; published online on November 27, 2021. Discussion period open until April 27, 2022; separate discussions must be submitted for individual papers. This paper is part of the ***Journal of Engineering Mechanics***, © ASCE, ISSN 0733-9399.

on the compaction. Man et al. (2022) recently developed a more realistic discrete-element model for compaction of hot asphalt mixtures, in which the composite particle model was used to simulate nonspherical aggregates. The interparticle contact law considered both the Hertizian–Mindlin contact between coarse aggregates and the lubrication action of the viscous asphalt binder and fine aggregates. By capturing the motion of each aggregate, the discrete modeling approach provides more insights into the mechanism of compaction process. However, the main drawback is the excessive computational cost, which makes it prohibitive for large-scale simulations.

In contrast to computational modeling, very limited efforts have been devoted to analytical modeling of asphalt compaction. Analytical modeling is advantageous in terms of computational efficiency. Meanwhile, it also provides an effective means for investigating the relations between the material properties and overall compactability of asphalt mixtures. In this study, we developed a one-dimensional (1D) nonlocal continuum model for gyratory compaction, based on the mesoscopic mechanism of granular compaction. The proposed model is calibrated and validated by a set of gyratory compaction tests on asphalt specimens of different heights.

Model Description

In gyratory compaction, the loose mixture is contained in a rigid cylindrical mold, of radius R. The top plate gyrates horizontally around the central axis at a constant angular velocity ω. The bottom plate is pushed vertically up under constant pressure P [Fig. 1(a)]. The mixture is compacted to a dense state under the combined compression and shear loading. Compaction deformation occurs in the vertical direction, although there is shear deformation in the horizontal direction. Therefore, we may model the compaction process by using a one-dimensional model, in which each material point represents a cross-section of the specimen, as shown in Fig. 1(b).

Mass Balance Equation

Let $x(X,t)$ denote the current position of the material point, which is located at X in the reference configuration, and $\rho(x,t)$ be the average density of the material of a cross-section at location x and time t. The local form of mass conservation can then be written as (Malvern 1969; Rudnicki 2015)

$$\frac{\mathrm{d}}{\mathrm{d}t}\left\{\rho[x(X,t),t]\frac{\partial x(X,t)}{\partial X}\right\}=0 \tag{1}$$

We define packing fraction ϕ as the volume ratio of aggregates and binder to the bulk volume of the mixture, and the air void ratio can be calculated by $1-\phi$. By this definition, ϕ can be computed as ρ/ρ_m, where ρ_m denotes the maximum possible density of the mixture, which corresponds to the case of $\phi=1$. Eq. (1) can be rewritten in terms of the packing fraction, that is

$$\frac{\mathrm{d}}{\mathrm{d}t}\left\{\phi[x(X,t),t]\frac{\partial x(X,t)}{\partial X}\right\}=0 \tag{2}$$

It is reasonable to consider that, for gyratory compaction, the initial packing fraction of the mixture is uniform because the effect of gravity is minimal; that is, $\phi(X,0)=\phi_0$. With this initial condition, Eq. (2) yields

$$\phi[x(X,t),t]\frac{\partial x(X,t)}{\partial X}=\phi_0 \tag{3}$$

Eq. (3) relates the current configuration of the specimen to the local packing fraction. To determine the current configuration, we need the second equation, which relates the packing fraction to the deformation state. Clearly, the relation between the packing fraction and deformation state must be tied to the mechanism of the compaction process.

In this study, we propose a model of the material point velocity $v(x,t)$. The compaction of asphalt mixture is driven by the rearrangement of aggregates in the viscous binder, which can be regarded as a process of transitions between different packing states (Yan et al. 2021b). During compaction, the external excitation (gyratory motion and compression) supplies the energy to the system for aggregate rearrangement and transition from a loose packing state to a denser one. Therefore, the material point velocity $v(x,t)$ can be related to the rate of the transition between different packing states.

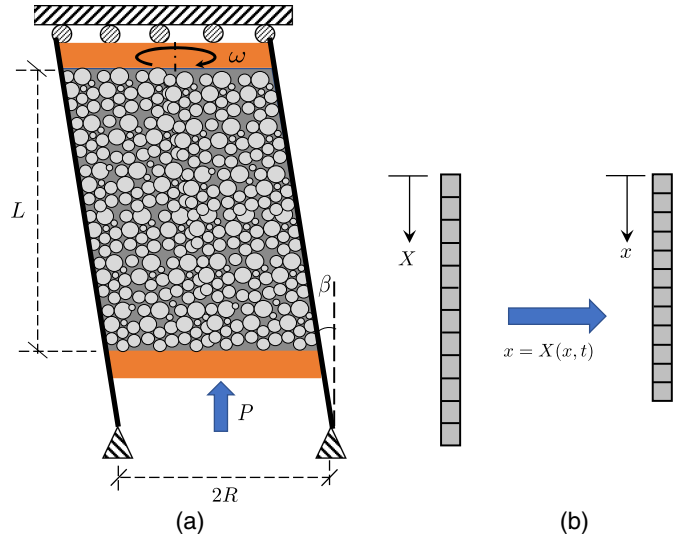

Fig. 1. Schematics of gyratory compaction of asphalt mixtures: (a) test setup; and (b) one-dimensional model.

Nonlocal Densification Model

Here we consider a cluster of aggregates, which has a height of l_0 and a cross-section the same as that of the gyratory compaction specimen. From the viewpoint of energy landscape, each packing state of the cluster (i.e., configuration of aggregate arrangement) can be considered a metastable state. The transition between metastable energy states has been studied extensively in statistical mechanics, (e.g., Kramers 1940; Risken 1989; Tadmor and Miller 2011). One well-known model is the transition rate theory, which leads to the Kramers equation for the rate of escape from a deep energy well (Kramers 1940). The Kramers model has been applied to study the general phenomena of state transition (Salamon et al. 1988). In the model, the frequency of the transition between two adjacent metastable states can be described by

$$f=f_0\exp(-U_a/E_s) \tag{4}$$

where f_0 = reference frequency; U_a = energy barrier across two adjacent states; and E_s = intrinsic energy of the system, which is referred to as the system energy that can activate the transition between adjacent states. For instance, when applying Eq. (4) to thermally activated process of nanoscale structures, one can consider E_s = thermal energy ($E_s=k_bT$, k_b = Boltzmann constant, and

T = absolute temperature) and U_a the activation barrier (Bazant and Le 2017).

We apply Eq. (4) to the transition between different packing states during gyratory compaction. Aggregate rearrangement is driven by mechanical loading, which is not a thermally activated process. Here we consider that the intrinsic energy of the cluster of aggregates is related to the gyratory motion, which induces shearing of the loose asphalt mixture. As an analogy to the thermal energy for thermally activated process, we consider E_s to be associated with the kinetic energy of the aggregates induced by the shearing motion, which can be expressed by

$$E_s = C\rho_a V_a \dot{\gamma}^2 d_a^2 \tag{5}$$

where C = constant; ρ_a = aggregate density; $\dot{\gamma}$ = shear rate induced by the gyration; d_a = average aggregate diameter; and V_a = volume of the aggregates in the cluster.

Consider the transition between two adjacent packing states. The absolute volume difference of these two states is denoted by δV [Fig. 2(a)]. This volume change is driven by the movement of the bottom plate. Therefore, the energy input by the vertical pressure is given by $P\delta V$. This energy input creates a bias of the energy landscape of the packing states. As shown in Fig. 2(b), the energy barrier for transitioning from a loose to dense state is lower than that for transitioning from a dense to loose state. The net frequency of the transition can be written as

$$\begin{aligned} f_V &= f_V^+ - f_V^- \\ &= f_0\left[\exp\left(-\frac{U_b - P\delta V/2}{E_s}\right) - \exp\left(-\frac{U_b + P\delta V/2}{E_s}\right)\right] \end{aligned} \tag{6}$$

$$= 2f_0 e^{-U_b/E_s}\sinh\left(\frac{P\delta V}{2E_s}\right) \tag{7}$$

where f_V^+ = frequency of transition from a loose to dense state; f_V^- = frequency of transition from a dense to loose state; and U_b = free energy barrier in absence of pressure P. Because compaction is a continuous process consisting of transitions between numerous packing states, we may consider $P\delta V \ll E_s$ and rewrite Eq. (7) as

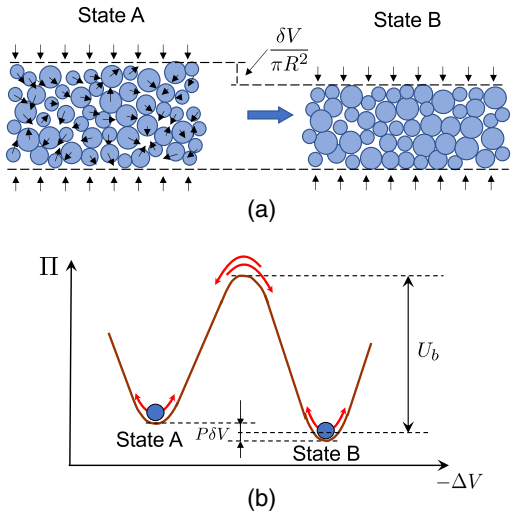

Fig. 2. (a) Schematic of aggregate rearrangement in a cluster; and (b) transition between adjacent packing states.

$$f_V \approx f_0 e^{-U_b/E_s}\frac{P\delta V}{E_s} \tag{8}$$

Consequently, the volumetric strain rate can then be expressed as

$$\dot{\epsilon}_V = -f_V \delta V/V_0 = -f_0\epsilon_0^2 e^{-U_b/E_s}\frac{PV_0}{E_s} \tag{9}$$

where $\epsilon_0 = -\delta V/V_0$ = volumetric strain induced by one state transition (the minus sign indicates that the cluster volume decreases during the transition); and V_0 = original volume of the cluster.

The energy barrier U_b is related to the packing fraction ϕ. It is expected that the rearrangement of aggregates will be easier when aggregates are loosely packed (e.g., ϕ is close to ϕ_0) and will become increasingly difficult as ϕ increases. Therefore, U_b must increase with the packing fraction. Meanwhile, the movement of one aggregate will cause the rearrangement of a group of neighborhood aggregates. This collective behavior is evidenced by the results of discrete-element simulations (Liu et al. 2017; Gong et al. 2018b, a; Liu et al. 2018; Man et al. 2022).

Within the framework of continuum modeling, the interaction of the neighboring aggregates can be represented by a nonlocal model. In general, there are two classes of nonlocal models, nonlocal integral and gradient models. In the integral model, the nonlocal quantity is calculated as a weighted average of the local quantities in the neighborhood, whereas in the gradient model, the nonlocal quantity is governed by a differential equation. It has been shown that in one dimension, the gradient model is equivalent to the integral model with a particular form of weighting function (Peerlings et al. 2001). Here we adopt an implicit gradient model in which the nonlocal packing fraction is governed by the following differential equation (Peerlings et al. 2001; Kamrin and Koval 2012; Bažant and Le 2017; Kamrin 2019):

$$\bar{\phi}(x,t) - \frac{l_a^2}{2}\frac{\partial^2\bar{\phi}(x,t)}{\partial x^2} = \phi(x,t) \tag{10}$$

where $\bar{\phi}(x,t)$ = nonlocal packing fraction of material point; $\phi(x,t)$ = local packing fraction of material point; and l_a = material characteristic length. Eq. (10) can be derived from the integral model by using the Taylor expansion to express the local quantities in the neighborhood (Peerlings et al. 2001; Bažant and Le 2017). The material length l_a controls the size of the nonlocal interaction zone. In the present model, it is natural to relate l_a to the cluster size l_0. Similar to nonlocal models for material damage (Bažant and Pijaudier-Cabot 1988; Bažant and Jirásek 2002), here we consider l_a proportional to the mean aggregate size d_a ($l_a = \eta d_a$). Furthermore, during the gyratory compaction, the rearrangement of aggregates and consequently the proportionality constant η are affected strongly by the viscous behavior of the binder as well as the contact properties of aggregates.

It is clear that Eq. (10) must be supplemented by the boundary conditions. For gyratory compaction, the rigid plates at two ends provide significant restraints to the motion of aggregates (Masad et al. 2002; Tashman et al. 2002; Thyagarajan et al. 2010). In the present model, this behavior is represented by two essential boundary conditions, that is

$$\bar{\phi}(0,t) = \bar{\phi}(L,t) = 1, \quad \text{for } t \geq 0 \tag{11}$$

Based on the foregoing discussion, we propose a simple relation between the energy barrier and the nonlocal packing fraction as

$$U_b = U_0 + U_1\langle\bar{\phi} - \phi_t\rangle^k \tag{12}$$

where $\langle x\rangle = \max(x, 0)$; and U_0, U_1, k, ϕ_t = constants. By substituting Eq. (12) into Eq. (9) and noting the one-dimensional nature of the present model, we obtain

$$\frac{\partial v(x,t)}{\partial x} = -C_1 P(x,t)\exp[-C_2\langle\bar{\phi}(x,t) - \phi_t\rangle^k] \tag{13}$$

where $v(x,t) = \partial x/\partial t$; $C_1 = f_0\epsilon_0^2 V_0/E_s \exp(-U_0/E_s)$; and $C_2 = U_1/E_s$. For a particular gyratory compaction test on a given asphalt mixture, we may consider C_1, C_2, k, and ϕ_t constants. In the model, we further impose a densification rate $\partial v(x,t)/\partial x$ to be zero if the local packing fraction reaches 1. This condition guarantees that the maximum packing fraction equals 1. A similar form of Eq. (13), but in a local framework, was used to describe the material-point velocity for modeling the density relaxation process of dry granular under tapping (Knight et al. 1995; Peng and Ohta 1998; Ben-Naim et al. 1998).

In Eq. (13), the local strain rate is related to the local pressure. Therefore, in principle, we would need to supplement Eq. (13) by an equilibrium equation. By neglecting the wall friction of the compactor and gravity, the present 1D model indicates that the pressure remain constant $P(x,t) = P$. Therefore, Eqs. (3) and (13) suffice for describing the behavior of the gyratory compaction in a simplified 1D setting.

Initial and Boundary Conditions and Numerical Solution

A finite-difference numerical scheme is used to solve Eqs. (3), (10), and (13). Because the space is discretized in the reference configuration, it is more convenient to write Eqs. (10) and (13) in the reference configuration using the chain rule, that is

$$\frac{\partial x(X,t)}{\partial X} = \frac{\phi_0}{\phi(X,t)} \tag{14}$$

$$\bar{\phi}(X,t) - \frac{l_a^2}{2}\left[\frac{\partial^2\bar{\phi}(X,t)}{\partial X^2}\left(\frac{\phi(X,t)}{\phi_0}\right)^2 - \frac{\partial\bar{\phi}(X,t)}{\partial X}\left(\frac{\partial^2 x}{\partial X^2}\right)\left(\frac{\phi(X,t)}{\phi_0}\right)^3\right] = \phi(X,t) \tag{15}$$

$$\frac{\partial v(X,t)}{\partial X} = -\frac{C_1 P\phi_0}{\phi(X,t)}\exp[-C_2\langle\bar{\phi}(X,t) - \phi_t\rangle^k] \tag{16}$$

In addition to the boundary condition of the nonlocal packing fraction [Eq. (11)], we also impose the boundary condition for the top plate ($X = 0$), where the vertical movement of the top plate is restrained

$$v(0,t) = v_0(t) = 0, \quad \text{for } t \geq 0 \tag{17}$$

$$x(0,t) = x_0(t) = 0, \quad \text{for } t \geq 0 \tag{18}$$

The initial condition of the system is given by $x(X,0) = X$.

In the numerical scheme, the reference domain $\Omega_0(X \in [0, L])$ is discretized into n equal intervals, and the nodal coordinates can be written as $X_i = i\Delta X(i = 0, 1, \ldots n)$, where ΔX = interval size. To facilitate the finite-difference scheme, a pseudonode X_{-1} is added at $X = -\Delta X$. Let Δt denote the time step.

Consider that we know all the nodal positions $x_i(t)$ at time t and now try to calculate the nodal position at time step $t + \Delta t$. In the present analysis, the spatial derivatives of any variable y are evaluated by finite differences: $\partial y/\partial X|_{X_i} \approx [y_i(t) - y_{i-1}(t)]/\Delta X$ and $\partial^2 y/\partial X^2|_{X_i} \approx [y_{i+1}(t) + y_{i-1}(t) - 2y_i(t)]/\Delta X^2$, where the subscript indicates the coordinate of the grid. By substituting these finite-difference approximations into Eqs. (14) to (19), we obtain

$$v_i(t + \Delta t) = \mathcal{F}_i[x_{-1}(t + \Delta t), x_0(t + \Delta t), \ldots, x_n(t + \Delta t)] \quad (i = 0, \ldots, n) \tag{19}$$

where the function $\mathcal{F}_i$ relates the nodal positions of all grids to the densification rate at grid i at time $t + \Delta t$. To ensure the stability of the solution, an implicit scheme is used to determine the new position of the node X_i, that is, $x_i(t + \Delta t) = x_i(t) + v_i(t + \Delta t)\Delta t$. By substituting the expression of $x_i(t + \Delta t)$ into Eq. (19), we obtain a system of equations from which we solve the new nodal position $x_i(t + \Delta t)$ by using the secant method.

Experimental Investigation

A set of gyratory compaction tests was conducted to calibrate and validate the model. The asphalt mixture was designed using the Superpave volumetric design method [AASHTO M 323 (AASHTO 2013)], with a target air-void ratio of 4% and a 20-year traffic level of 3–10 million equivalent single axle load (ESAL). The mixture had a binder content of 5.8% by weight. The performance grade of the binder was PG 58H-28 according to AASHTO M 332 (AASHTO 2020c). The theoretical maximum density of the mixture ρ_m was measured to be 2.495 g/cm^3 based on AASHTO T 209 (AASHTO 2020b). The nominal maximum aggregate size of this mixture was 9.5 mm. The aggregate gradation of the mixture is listed in Table 1.

The salient feature of the present model is the consideration of nonlocality, which naturally involves a material length. A natural consequence is that the predicted compaction behavior would exhibit a strong size effect. To examine this size effect, three specimen sizes were used in the experiments. The sizes of specimens were controlled by the weight of the loose mixture used to compact the cylindrical specimens: 2.5, 3.5, and 4.5 kg. For each specimen size, two replicates were tested.

The standard method for gyratory compaction, AASHTO T 312 (AASHTO 2019), was followed. The loose mixture and cylindrical gyratory mold were first heated in the oven at the compaction temperature. The mixture was then poured into the gyratory mold and compacted using the gyratory compactor of a diameter of 150 mm. During compaction, the height of the specimen h was recorded after each gyration. In this research, all specimens were subjected to 200 gyrations; the compaction temperature was 130°C. According to AASHTO T 312, the external pressure P was 600 kPa, the gyration angle β was 1.16°, and the rate of gyration ω was 30 times per minute.

Table 1. Aggregate gradation

Sieve size (mm)	Percent passing (%)
12.5	100
9.5	97
4.75	75
2.36	54
1.18	36
0.6	25
0.3	15
0.15	7
0.075	4.8

Table 2. Average bulk density of compacted specimens

Specimen weight (kg)	Replicate	ρ^f_{ave} (g/cm^3)
2.5	1	2.391
	2	2.382
3.5	1	2.425
	2	2.430
4.5	1	2.438
	2	2.435

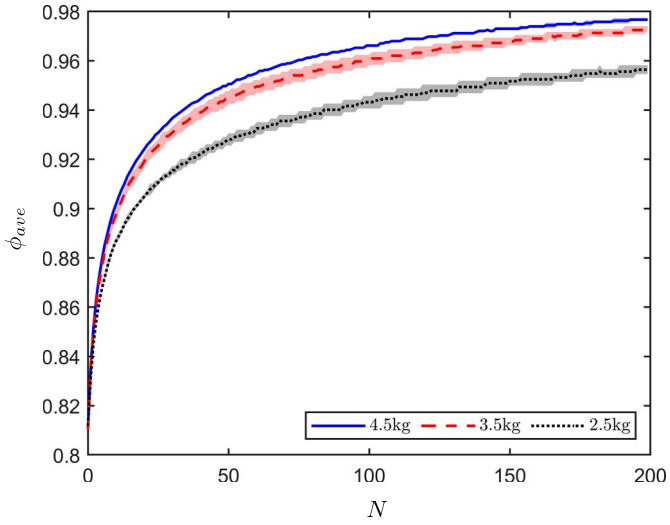

Fig. 3. Experimental compaction curves of different-sized specimens (lines denote the average response, and shaded areas denote the scatter of the data).

The temperature of the specimens was measured before and after the compaction. At the beginning of the compaction, all specimens had a similar temperature, which was slightly lower than the oven temperature, 130°C. During the compaction process, the temperature of the specimen dropped. It was observed that small specimens experienced a more pronounced temperature drop. The temperature of 2.5-kg specimens decreased from 128°C to 96°C, whereas for 4.5 kg specimens, the temperature dropped from 125.5°C to 105.7°C. This difference in temperature change is due to the fact that small specimens have a larger surface-to-volume ratio, which allows more heat dissipation.

At the end of gyratory compaction, the final bulk density of the compacted specimen ρ^f_{ave} was measured according to AASHTO T 166 (AASHTO 2020a). The results are shown in Table 2. Based on the measured evolution of specimen height, the average bulk density of the specimen at the Nth gyration $\rho_{\text{ave}}(N)$ can be calculated as

$$\rho_{\text{ave}}(N) = \rho^f_{\text{ave}} \frac{h^f}{h(N)} \tag{20}$$

where $h(N)$ = specimen height at the Nth gyration; and h^f = final height of the specimen. The average packing fraction of the specimen at the Nth gyration $\phi_{\text{ave}}(N)$ can then be calculated as

$$\phi_{\text{ave}}(N) = \frac{\rho_{\text{ave}}(N)}{\rho_m} \tag{21}$$

Fig. 3 shows the relationship between the average packing fraction ϕ_{ave} and the number of gyrations N, which is referred to as the compaction curve. It is seen that, for all specimens, the compaction curves featured the same behavior. The packing fraction increased quickly during the early stage of the compaction ($0 < N < 50$), and in the subsequent gyrations, the increase in packing fraction occurred at a much slower rate. This behavior was well expected because it becomes more difficult to rearrange the aggregates at a higher packing fraction.

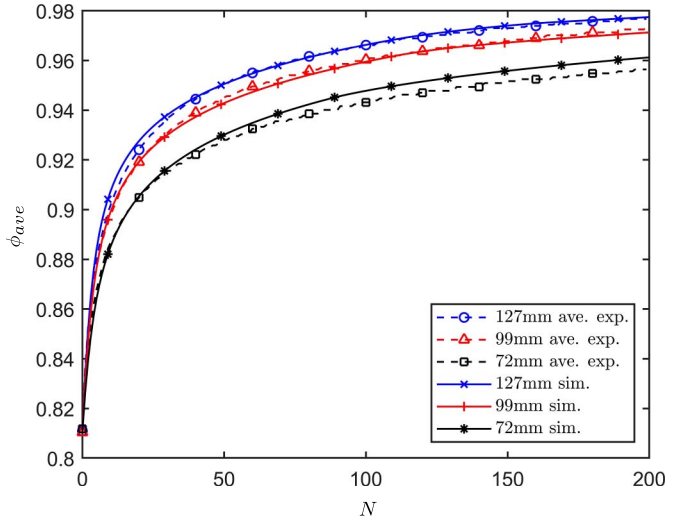

Fig. 4. Comparison between the measured and simulated compaction curves of specimens of different sizes.

The notable result of the present experiment is that the specimen size has a profound effect on the compaction curve. As shown in Fig. 3, for a given number of gyrations, the packing fraction increased with specimen size. This indicates that large specimens are easier to compact compared to small specimens. The difference in compaction curve between specimens of different sizes occurred mainly at the initial stage of the compaction ($0 < N < 50$). In the later stage of the compaction, this difference remained almost unchanged. During the early stage of the compaction, the difference in temperature drop in specimens of different sizes would not be significant. Therefore, we may conclude that the difference in the measured compaction curves for specimen of different sizes is not due to the temperature effect.

Simulation of Gyratory Compaction Experiments

The present model was used to simulate the aforementioned compaction experiments. The initial packing fraction and specimen height were measured for each specimen prior to the experiments: $\phi_0 = 0.81$ and $L = 127$, 99, and 72 mm for 4.5-kg, 3.5-kg, and 2.5-kg specimens, respectively. The remaining parameters, C_1, C_2, k, l_a, and ϕ_t, need to be calibrated. Due to the nonlocality, one cannot uniquely determine these parameters by the optimum fitting of the compaction curve of one specimen size. In this study, the model parameters were calibrated by fitting of the measured compaction curves of 127-mm and 99-mm specimens, and the calibrated model was then used to predict the compaction curve of 72-mm specimens.

Fig. 4 shows the optimum fitting of the experimental compaction curves of 127-mm and 99-mm specimens by the present model. It is seen that the model matches well the experimental results of these two different size specimens. For the fitting of the 127-mm specimen, the root mean square error (RMSE) was 0.0016, and the

coefficient of determination (R^2 value) was 99.55%. For the fitting of the 99-mm specimen, the RMSE was 0.0014, and the R^2 value was 99.69%. The fitting yielded the following values of the model parameters: $l_a = 20$ mm, $C_1 = 0.033$ MPa^{-1} s^{-1}, $C_2 = 341$, $k = 2.5$, and $\phi_t = 0.8$. Note that the calibrated nonlocal influence length is about twice the nominal maximum aggregate size.

These fitted parameters were then used to simulate the gyratory compaction of the 72-mm specimen. As shown in Fig. 4, the prediction was in good agreement with the measured compaction curve, with the RMSE being 0.0039 and the R^2 value being 96.94%. The essential feature of the present model is its ability to capture the effect of specimen size on the compaction curve. This is the key consequence of employing the nonlocal model, which contains a characteristic material length scale invariant with the specimen size. The effect of nonlocality on the compaction behavior will be further discussed in the next section.

A common feature of the compaction curve is that the specimen first exhibits a high compaction rate, which is indicated by the slope of the compaction curve. As the compaction process proceeds, the compaction rate decreases significantly, and the compaction curve flattens eventually. This collective behavior is well captured by Eq. (13) of the present model, which predicts a decreasing local densification rate for an increasing packing fraction.

In addition to compaction curves, the model also simulates the evolution of packing fraction profiles, as shown in Figs. 5(a–c) for the three different specimen sizes. It can be seen that for all specimen sizes, as the number of gyrations increased, the packing fraction profile evolved gradually to a nonuniform distribution, which featured a low local packing fraction near the specimen ends and a relatively high local packing fraction in the middle. Such a spatial distribution of local packing fraction has been observed in previous experimental studies (Masad et al. 2002; Tashman et al. 2002; Masad and Button 2004; Thyagarajan et al. 2010) and discrete element simulations (Chen et al. 2013).

The emergence of the nonuniform distribution of the local packing fraction can be attributed to the restriction of the rigid loading plates on the aggregate rearrangement and the nonlocal effect. The movement of aggregates near the two ends was significantly restrained by the loading plates, whereas this restraint effect gradually faded for aggregates away from the ends. In the present model, the effect of the rigid plates was captured by the nonlocal boundary condition [Eq. (11)], which imposed a very low densification rate at the

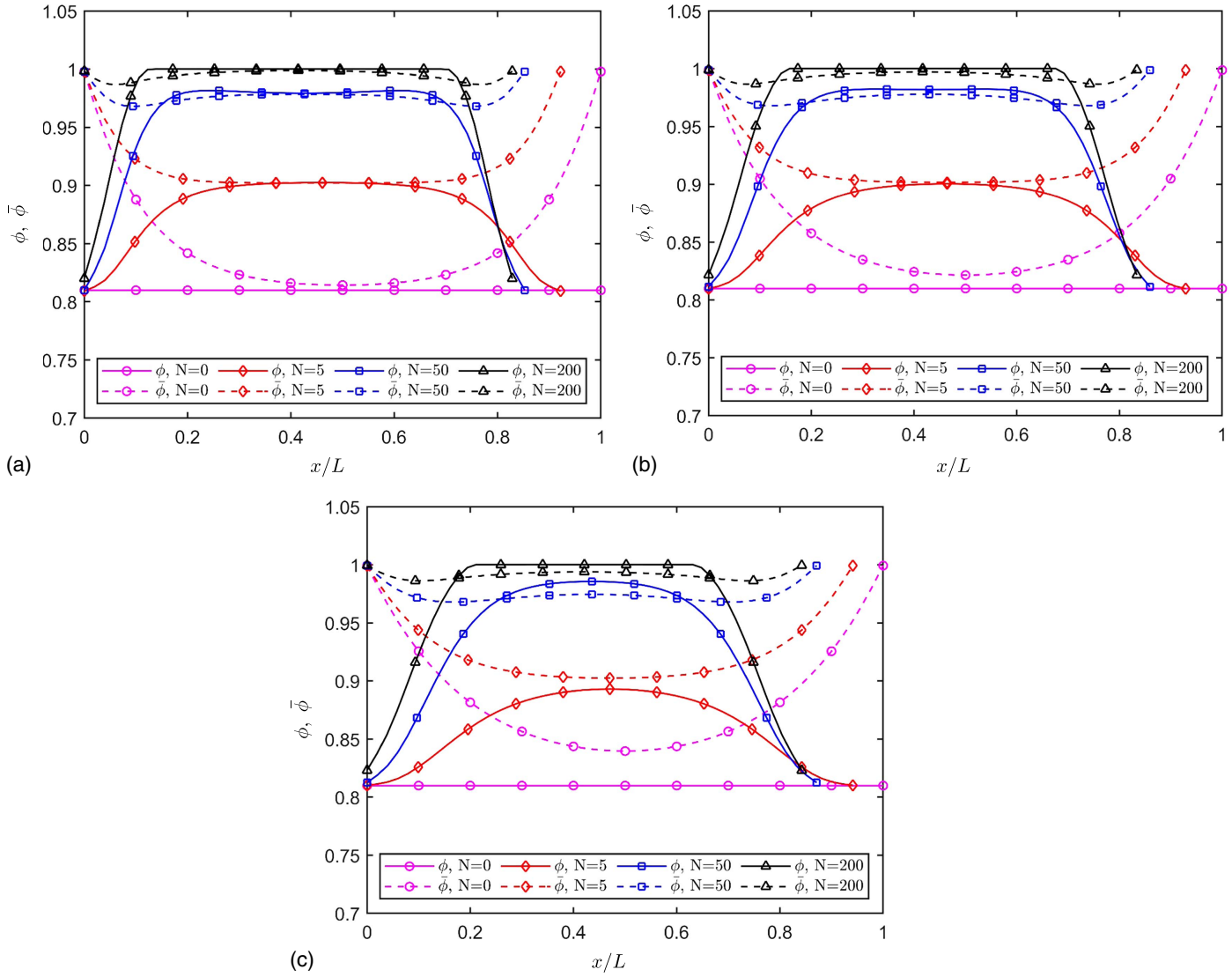

Fig. 5. Simulated evolution of local and nonlocal packing fraction profiles of specimens of different sizes: (a) 127-mm specimen; (b) 99-mm specimen; and (c) 72-mm specimen.

J. Eng. Mech., 2022, 148(2): 04021144

specimen ends. The gradual fading of this boundary effect toward the middle was described by the nonlocal model, where the nonlocal length governed how fast the restrain effect of the rigid plates disappeared as we moved away from the two ends. The model predicted a decreasing nonlocal packing fraction from the two ends toward the middle, as shown in Figs. 5(a–c). This behavior implies that the densification rate increases from the two ends toward the middle.

Based on the simulated spatial distribution of ϕ and $\bar{\phi}$ [Figs. 5(a–c)], we can divide the specimen into two parts: (1) a transition region occurring near the two ends, in which the local packing fraction showed a considerable increase, and (2) a stable region in the middle part, in which the local packing fraction exhibited almost a constant value. The foregoing discussion indicates that the material in the transition region was strongly affected by the boundary effect, whereas the material in the stable region was less affected.

Comparison between Figs. 5(a–c) reveals a strong effect of specimen size on the spatial distribution of both local and nonlocal packing fractions. It is seen that the ratio of the transition region to the entire specimen size decreased as the specimen size increased. The size of the transition region can be understood as the size range of the material that is affected by the rigid plates. In the present model, this size is intimately related to the nonlocal length scale l_a. In fact, the absolute size of the transition region for all specimen sizes was almost a constant. On the other hand, the local packing fraction of the stable region was almost a constant for all specimens. This implies that, at a certain number of gyrations, large specimens would exhibit a higher average local packing fraction, which explains the size effect observed in Fig. 4.

Parametric Analysis

Nonlocal Averaging Length Scale

The foregoing discussion reveals the critical role of nonlocality in the prediction of the compaction behavior of asphalt mixtures. In a 1D setting, the extent of the nonlocal effect can be described by the length ratio l_a/L. Therefore, it is naturally expected that, for a given mixture, specimens of different sizes would exhibit different compaction behaviors. To further investigate the effect of nonlocality on the compaction behavior, we repeated the simulation for a wide range of l_a/L values ($l_a/L = 0, 0.05, 0.1, 0.15, 0.2, 0.25, 0.3$) while the other parameters were kept unchanged. We simulated the compaction behavior for 50 gyrations.

Fig. 6 compares the simulated compaction curves for these six cases of l_a/L. It is seen that, as l_a/L decreased, the model predicted an increased compatibility over the entire compaction process. Fig. 7 presents the packing fraction profile at 50 gyrations. It is seen that, for small values of l_a/L, the transition region became negligible. Therefore, the specimen exhibited a lower overall nonlocal packing fraction and consequently a higher densification rate and increase in compatibility. As l_a/L decreased to zero, the compaction curve converged in a limiting form corresponding to the solution of the local model.

We denote the size of the transition region by l_m. Fig. 8 presents the relationship between l_m and l_a. It is seen that, when $l_a < 0.25L$, we have $l_m \approx 2l_a$, which implies that for a given mixture (given l_a),

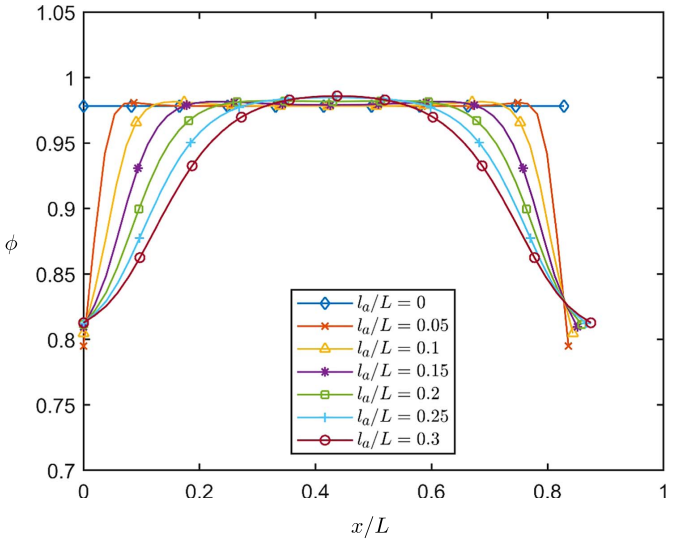

Fig. 7. Effect of nominalized nonlocal length scale l_a/L on the final distribution of the local packing fraction.

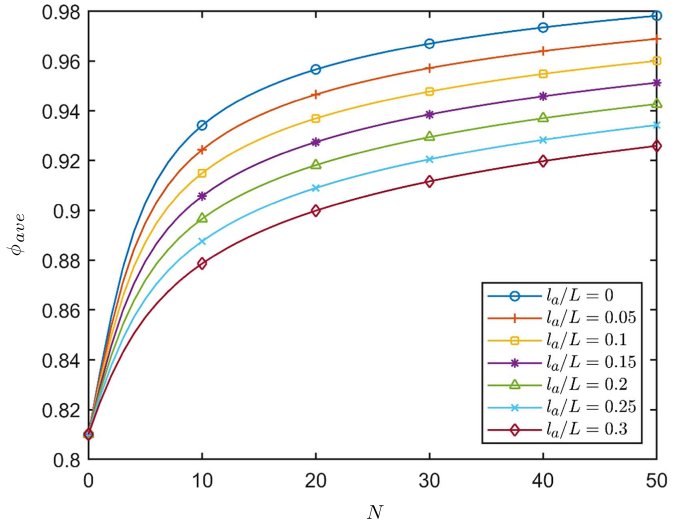

Fig. 6. Effect of nominalized nonlocal length scale l_a/L on the compaction curve.

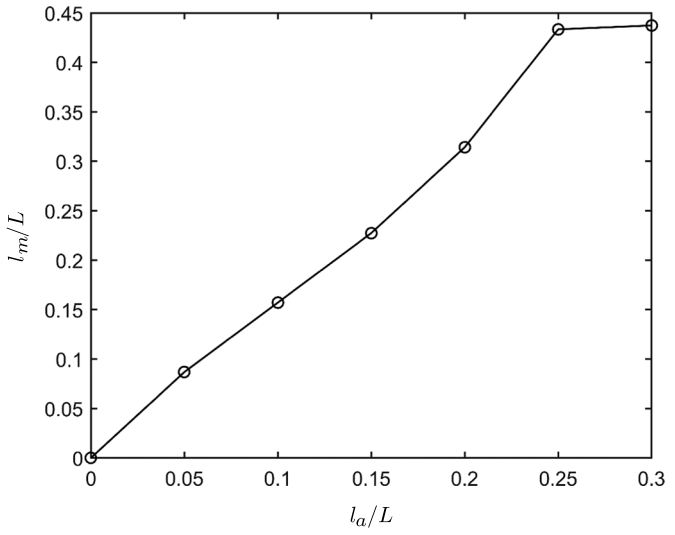

Fig. 8. Relationship between l_m/L and l_a/L.

Table 3. Parameters for investigation of the effect of C_1, C_2, and k

Set	C_1 (MPa^{-1} s^{-1})	C_2	k
1	0.01, 0.02, 0.03, 0.04, 0.05, 0.06	341	2.5
2	0.033	200, 300, 400, 500, 600, 700	2.5
3	0.033	341	1.5, 2.0, 2.5, 3.0, 3.5, 4.0

the size of the transition region is independent of the specimen size. However, when $l_a > 0.25L$, the size of transition region is about half of the specimen. In this case, l_m is proportional to the specimen size. This is because, when the nonlocal length is sufficiently large, the entire specimen would be affected by the boundary, and therefore the stable region disappears. In this limiting case we have $l_m/L = 0.5$.

The foregoing discussion of the nonlocal effect also implies the influence of aggregate size on the compactability of the gyratory compaction specimen. Because the nonlocal averaging length is proportional to the maximum aggregate size, it is clear that the specimen with a large aggregate size would exhibit a low compactability, which has been observed experimentally (Dan et al. 2020). In addition to the maximum aggregate size, the aggregate gradation could also influence the nonlocal averaging length. Such dependence has not been studied so far. Nevertheless, if size effect experiments on gyratory compaction on specimens made of different aggregate gradations were available, the present model could be used to explore the relation between the nonlocality and the characteristics of aggregate gradation described by some existing methods such as the Bailey method and the maximum density line (Leiva and West 2008; Vavrik et al. 2002).

Parameters C_1, C_2, and k

Parameters C_1, C_2, and k influence the compaction process through the densification model [Eq. (13)]. These parameters are closely related to the material properties and gyratory motion. Table 3 shows the three sets of simulation parameters for investigating the effects of C_1, C_2, and k on the overall compaction curve. In this set of parametric studies, we consider $l_a/L = 0.15$ and $\phi_t = 0.80$.

Figs. 9(a–c) show the effects of the parameters C_1, C_2, and k on the densification model, respectively. It is seen that C_1 has a

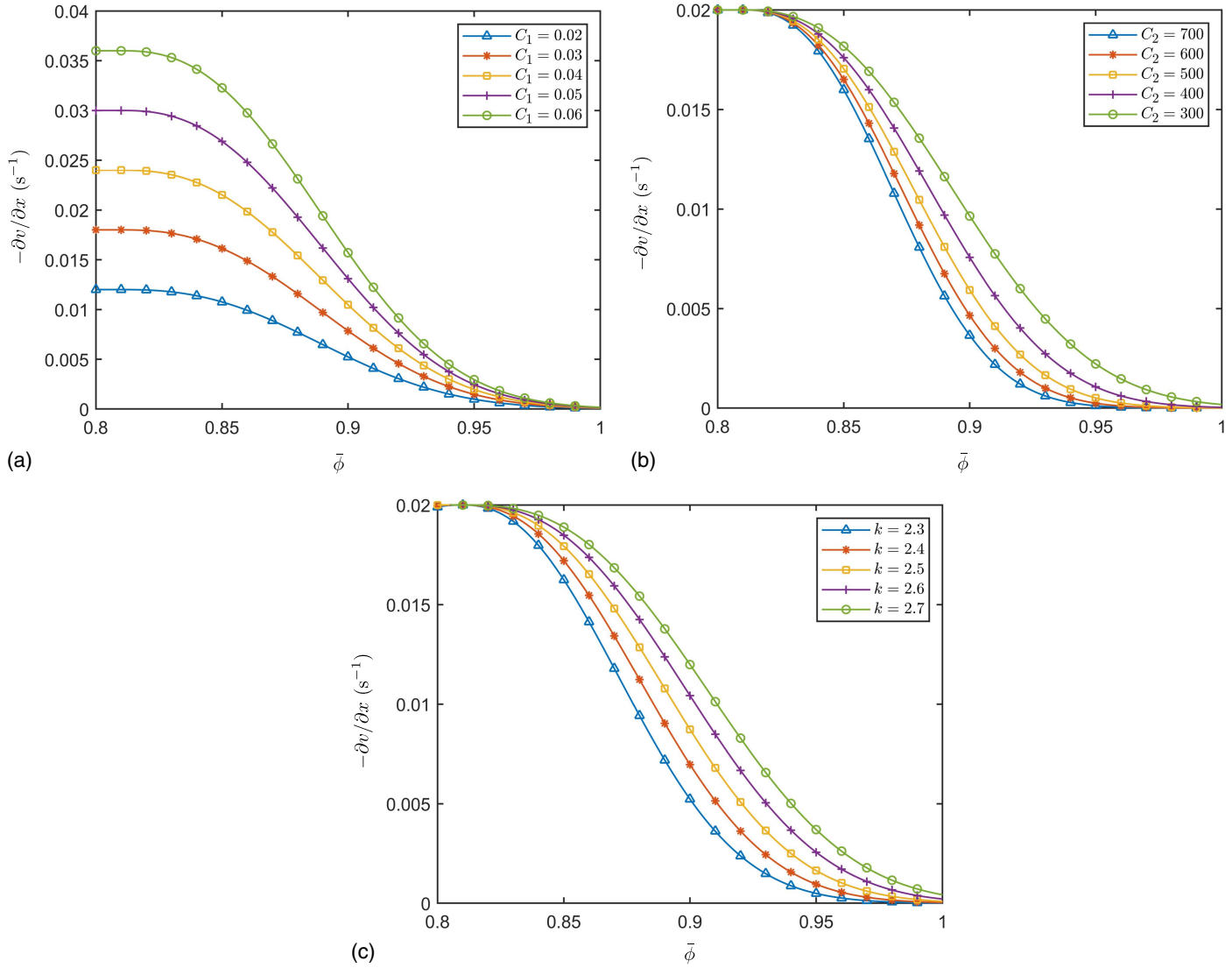

Fig. 9. Effects of model parameters on the local densification rate: (a) parameter C_1; (b) parameter C_2; and (c) parameter k.

J. Eng. Mech., 2022, 148(2): 04021144

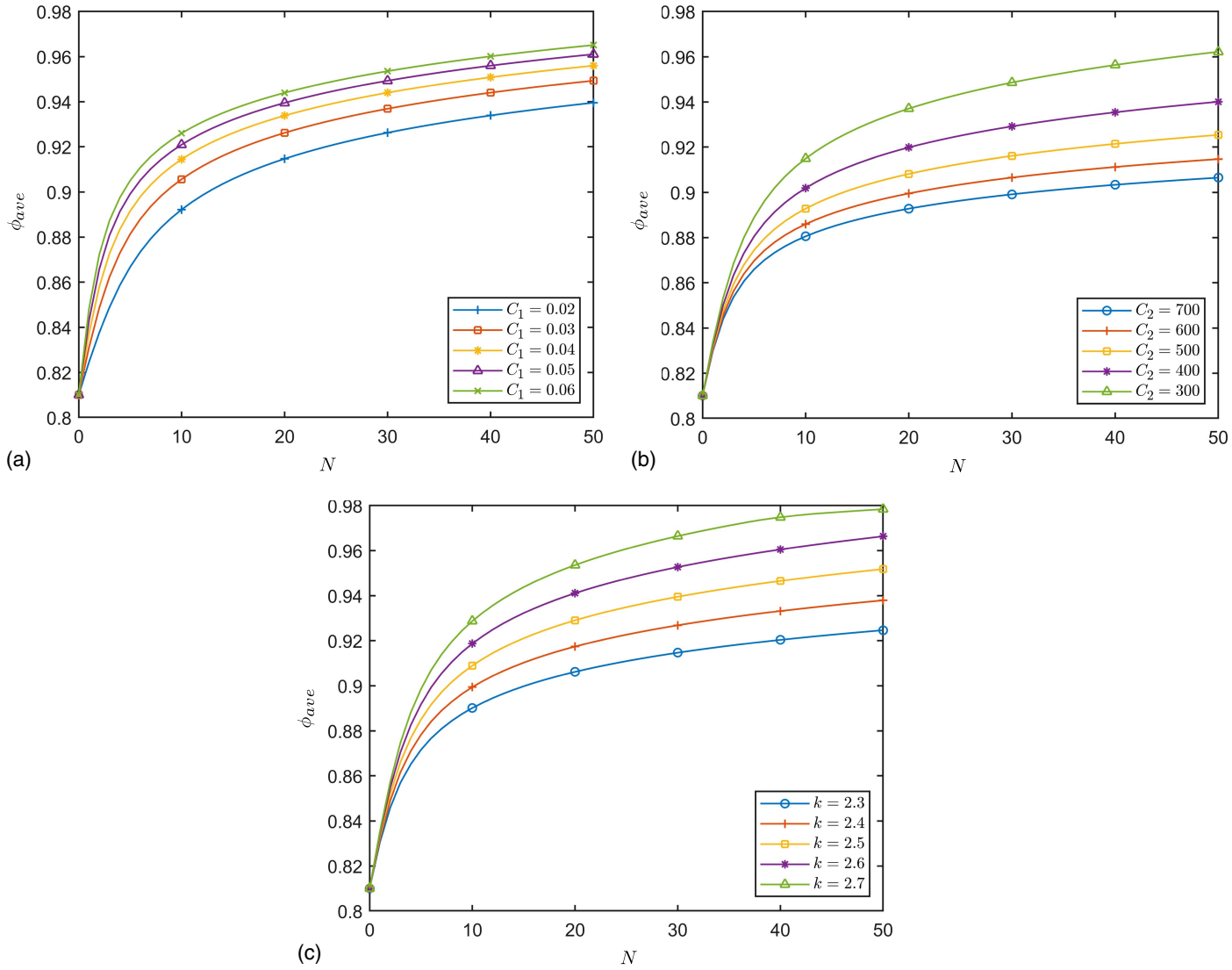

Fig. 10. Effects of model parameters on the compaction curve: (a) parameter C_1; (b) parameter C_2; and (c) parameter k.

significant influence on the densification rate when the nonlocal packing fraction $\bar{\phi}$ is close to ϕ_t. As $\bar{\phi}$ increased, the effect of C_1 on the densification rate attenuated. This behavior is reflected in Fig. 10(a), which shows that a larger value of C_1 led to a significant increase in the initial compaction rate, whereas the compaction rate during the later stage of the process was not affected by the parameter C_1.

In contrast to C_1, both C_2 and k had a pronounced effect on the densification rate for intermediate values of $\bar{\phi}$ [Figs. 9(b and c)]. Figs. 10(b and c) show the effects of C_2 and k on the compaction curve. It is seen that the compactability improved when C_2 decreased or k increased. As indicated by Figs. 9(b and c), the initial compaction rate was not affected by parameters C_2 and k. These parameters had a strong influence on the intermediate stage of the compaction process. Figs. 10(b and c) also show that, as compared to C_2, parameter k had a stronger effect on the compaction curve.

It is worthwhile to discuss the physical significance of the parameters C_1, C_2, and k in terms of their relation to the loading conditions and material properties. Based on Eq. (13), C_1 and C_2 are related to the kinetic energy E_s of the aggregates in the cluster. For a given material, E_s is governed by the gyratory motion, which can be controlled by the gyratory angle and speed. An increase in either gyratory angle or speed would lead to an increase in E_s and therefore an increase in C_1 and decrease in C_2. Therefore, the model predicts that both increases in gyratory angle and speed will accelerate the compaction process, which is consistent with the experimental observations (Tashman et al. 2001; Khan et al. 1998).

Meanwhile, C_1, C_2, and k also manifest the effect of material properties on the compactability of the mixture. It is widely accepted that the viscosity of the binder is a key factor for the compaction process of an asphalt mixture. In the present model, a higher binder viscosity implies a higher initial free energy barrier U_0 of aggregate rearrangements and a more significant increase in the energy barrier due to the increase in packing fraction (i.e., a higher value of U_1 and a lower value of k) and meanwhile a lower reference frequency f_0 of transition between two adjacent packing states. This indicates a decrease in C_1 and k and an increase in C_2, which leads to a decrease in densification rate and lower compatibility. Because the binder viscosity increased with decreasing temperature, the predicted effect of binder viscosity can also be used to explain the temperature effect on the compaction process.

In addition to the viscosity of the binder, the angularity of the aggregates has a profound influence on compactability (Leiva and

West 2008; Stakston et al. 2002; Delgadillo and Bahia 2008), and different experimental methods have been developed to measure the angularity [AASHTO T 304 (AASHTO 2017); ASTM D5821 (ASTM 2017)]. The present model predicts a similar effect of aggregate angularity on compactability as that of binder viscosity. Large angularity will lead to a lower value of f_0 and a higher and steeper increasing U_b, which consequently decelerates the compaction process, which has been observed experimentally (Leiva and West 2008; Stakston et al. 2002; Delgadillo and Bahia 2008). Similarly, the present model also explains the effect of the content of asphalt binder on compaction. The increase in asphalt binder content increases the thickness of asphalt film coating aggregates and thus provides an effect similar to reducing aggregate angularity. Therefore, increasing asphalt binder content would accelerate the compaction process.

It should be mentioned that C_1, C_2, and k may also depend on other properties, such as aggregate gradation. It is clear that a desirable aggregate gradation would correspond to a low free energy barrier and a high reference frequency of transition. Therefore, it is expected that the effect of aggregate gradation would be qualitatively similar to those of binder viscosity and aggregate angularity. The quantitative relation between the characteristic of aggregate gradation and free energy barrier and reference frequency could be determined through optimum fitting of the measured compaction curves by the present model.

Potential Applications

It is worthwhile to discuss the potential applications of the present model. The model provides an effective means to calculate the gyratory compaction curve. If the gyratory compaction curves of specimens of different heights are available for different mixtures, one can leverage modern machine learning techniques to establish the relationship between the model parameters and material composition (i.e., asphalt binder viscosity, aggregate angularity, and aggregate gradation). With the present model, this relationship will lead to a quantitative understanding of the underlying dependence of the characteristics of compaction curves on the material composition, which is critical for asphalt mix design to achieve the desired compactability of the mixture.

The model also provides a qualitative explanation of the effects of lift thickness and aggregate size on the field compaction, which has been observed in practice (McDaniel 2019). Based on the present model, the dependence of compaction performance on the lift thickness and aggregate size can be understood from the size effect on the gyratory compaction performance, a necessary consequence of the nonlocal model. However, in order to quantitatively predict the effect of lift thickness and aggregate size on the field compaction, one needs to relate the gyratory compaction to field compaction, which requires further investigation.

Conclusion

A one-dimensional nonlocal model is developed to simulate the gyratory compaction of asphalt mixtures. The model is formulated by combining the local mass balance law and a densification model for a cluster of aggregates. The densification model relates the transition rate between adjacent states to the energy inputs by the gyratory motion and compression as well as to the nonlocal packing fraction.

The model predicts an intricate effect of specimen height on the overall compaction curve. It shows that, for a given number of gyrations, the average packing fraction of the specimen decreases as the specimen height decreases. Meanwhile, the final spatial distribution of local packing fraction is also strongly dependent on the specimen height. The predicted size dependence of compaction behavior can be explained by the nonlocality of the densification rate.

A set of gyratory compaction tests is performed on hot asphalt mixture specimens of different heights. The test results show that the compaction curve is strongly dependent on the specimen height. The comparison between the model prediction and experimental results validates the present model, which demonstrates the critical role of nonlocality in the continuum modeling of gyratory compaction.

Through a set of parametric studies, it is shown that the nonlocal length scale plays a critical role in determining the spatial distribution of the local packing fraction and consequently the overall compaction curve. The model parameters can be related to the setup of the gyratory compaction test and the material properties, such as the binder viscosity, angularity of aggregates, and aggregate gradation. The model qualitatively predicts the effect of material properties on the compaction behavior, which are consistent with existing experimental observation. A more extensive experimental investigation would be required to establish the quantitative relations between these properties and compatibility.

Data Availability Statement

The computer code and experimental data generated from the study are available from the corresponding author by request.

Acknowledgments

The authors gratefully acknowledge the support under grant 100325 WO106 to the University of Minnesota from the Minnesota Department of Transportation.

References

AASHTO. 2013. *Standard specification for Superpave volumetric mix design*. AASHTO M 323. Washington, DC: AASHTO.

AASHTO. 2017. *Uncompacted void content of fine aggregate*. AASHTO T 304. Washington, DC: AASHTO.

AASHTO. 2019. *Standard method of test for preparing and determining the density of asphalt mixture specimens by means of the Superpave gyratory compactor.* AASHTO T 312. Washington, DC: AASHTO.

AASHTO. 2020a. *Standard method of test for bulk specific gravity (GMB) of compacted asphalt mixtures using saturated surface-dry specimens*. AASHTO T 166. Washington, DC: AASHTO.

AASHTO. 2020b. *Standard method of test for theoretical maximum specific gravity (GMM) and density of asphalt mixtures*. AASHTO T 209. Washington, DC: AASHTO.

AASHTO. 2020c. *Standard specification for performance-graded asphalt binder using multiple stress creep recovery (MSCR) test*. AASHTO M 332. Washington, DC: AASHTO.

Archilla, A., and S. Madanat. 2001. "Statistical model of pavement rutting in asphalt concrete mixes." *Transp. Res. Rec.* 1764 (1): 70–77. https://doi.org/10.3141/1764-08.

ASTM. 2017. *Standard test method for determining the percentage of fractured particles in coarse aggregate*. ASTM D5821. West Conshohocken, PA: ASTM.

Bažant, Z. P., and M. Jirásek. 2002. "Nonlocal integral formulations of plasticity and damage: Survey of progress." *J. Eng. Mech.* 128 (11): 1119–1149. https://doi.org/10.1061/(ASCE)0733-9399(2002)128:11(1119).

Bažant, Z. P., and J.-L. Le. 2017. *Probabilistic mechanics of quasi-brittle structures: Strength, lifetime, and size effect*. Cambridge, UK: Cambridge University Press.

Bažant, Z. P., and G. Pijaudier-Cabot. 1988. "Nonlocal continuum damage, localization instability and convergence." *J. Appl. Mech.* 55 (Jun): 287–293.

Ben-Naim, E., J. B. Knight, E. R. Nowak, H. M. Jaeger, and S. R. Nagel. 1998. "Slow relaxation in granular compaction." *Physica D* 123 (1–4): 380–385. https://doi.org/10.1016/S0167-2789(98)00136-5.

Chen, J., B. Huang, and X. Shu. 2013. "Air-void distribution analysis of asphalt mixture using discrete element method." *J. Mater. Civ. Eng.* 25 (10): 137–1385. https://doi.org/10.1061/(ASCE)MT.1943-5533.0000661.

Chen, J., B. Huang, X. Shu, and C. Hu. 2014. "DEM simulation of laboratory compaction of asphalt mixtures using an open source code." *J. Mater. Civ. Eng.* 27 (3): 04014130. https://doi.org/10.1061/(ASCE)MT.1943-5533.0001069.

Consuegra, A., D. N. Little, H. Von Quintus, and J. L. Burati. 1989. "Comparative evaluation of laboratory compaction devices based on their ability to produce mixtures with engineering properties similar to those produced in the field." *Transp. Res. Rec.* 1228 (1): 80–87.

Cooley, L. A., E. R. Brown, and S. Maghsoodloo. 2001. "Developing critical field permeability and pavement density values for coarse-graded Superpave pavements." *Transp. Res. Rec.* 1761 (1): 41–49. https://doi.org/10.3141/1761-06.

Dan, H.-C., D. Yang, L. Zhao, S. Wang, and Z. Zhang. 2020. "Meso-scale study on compaction characteristics of asphalt mixtures in Superpave gyratory compaction using smartrock sensors." *Constr. Build. Mater.* 262 (Nov): 120874. https://doi.org/10.1016/j.conbuildmat.2020.120874.

Delgadillo, R., and H. U. Bahia. 2008. "Effects of temperature and pressure on hot mixed asphalt compaction: Field and laboratory study." *J. Mater. Civ. Eng.* 20 (6): 440–448. https://doi.org/10.1061/(ASCE)0899-1561(2008)20:6(440).

Dessouky, S., E. Masad, and F. Bayomy. 2004. "Prediction of hot mix asphalt stability using the Superpave gyratory compactor." *J. Mater. Civ. Eng.* 16 (6): 578–587. https://doi.org/10.1061/(ASCE)0899-1561(2004)16:6(578).

Faheem, A. F., H. U. Bahia, and H. Ajideh. 2005. "Estimating results of a proposed simple performance test for hot-mix asphalt from Superpave gyratory compactor results." *Transp. Res. Rec.* 1929 (1): 104–113. https://doi.org/10.1177/0361198105192900113.

Finn, F. N., and J. A. Epps. 1980. *Compaction of hot mix asphalt concrete*. Austin, TX: Texas Transportation Institute.

Gong, F., Y. Liu, X. Zhou, and Z. You. 2018a. "Lab assessment and discrete element modeling of asphalt mixture during compaction with elongated and flat coarse aggregates." *Constr. Build. Mater.* 182 (Sep): 573–579. https://doi.org/10.1016/j.conbuildmat.2018.06.059.

Gong, F., X. Zhou, Z. You, Y. Liu, and S. Chen. 2018b. "Using discrete element models to track movement of coarse aggregates during compaction of asphalt mixture." *Constr. Build. Mater.* 189 (Nov): 338–351. https://doi.org/10.1016/j.conbuildmat.2018.08.133.

Harman, T., J. R. Bukowski, F. Moutier, G. A. Huber, and R. McGennis. 2002. "History and future challenges of gyratory compaction: 1939 to 2001." *Transp. Res. Rec.* 1789 (1): 200–207. https://doi.org/10.3141/1789-22.

Hughes, C. S. 1989. "Compaction of asphalt pavement." In *National cooperative highway research program synthesis of highway practice*. Washington, DC: Transportation Research Board.

Kamrin, K. 2019. "Non-locality in granular flow: Phenomenology and modeling approaches." *Front. Phys.* 7 (Aug): 1–7. https://doi.org/10.3389/fphy.2019.00116.

Kamrin, K., and G. Koval. 2012. "Nonlocal constitutive relation for steady granular flow." *Phys. Rev. Lett.* 108 (17): 178301. https://doi.org/10.1103/PhysRevLett.108.178301.

Karimi, M. M., M. K. Darabi, and N. Tabatabaee. 2019. "A thermodynamic-based large deformation viscoplastic constitutive relationship for asphalt concrete compaction." *Int. J. Solids Struct.* 165 (Jun): 192–216. https://doi.org/10.1016/j.ijsolstr.2019.01.016.

Khan, Z. A., H. I. A. Wahab, I. Asi, and R. Ramadhan. 1998. "Comparative study of asphalt concrete laboratory compaction methods to simulate field compaction." *Constr. Build. Mater.* 12 (6–7): 373–384. https://doi.org/10.1016/S0950-0618(98)00015-4.

Knight, J. B., C. G. Fandrich, C. N. Lau, H. M. Jaeger, and S. R. Nagel. 1995. "Density relaxation in a vibrated granular material." *Phys. Rev. E* 51 (5): 3957. https://doi.org/10.1103/PhysRevE.51.3957.

Koneru, S., E. Masad, and K. R. Rajagopal. 2008. "A thermomechanical framework for modeling the compaction of asphalt mixes." *Mech. Mater.* 40 (10): 846–864. https://doi.org/10.1016/j.mechmat.2008.03.008.

Kramers, H. A. 1940. "Brownian motion in a field of force and the diffusion model of chemical reaction." *Physica* 7 (4): 284–304. https://doi.org/10.1016/S0031-8914(40)90098-2.

Leiva, F., and R. C. West. 2008. "Analysis of hot-mix asphalt lab compactability using lab compaction parameters and mix characteristics." *Transp. Res. Rec.* 2057 (1): 89–98. https://doi.org/10.3141/2057-11.

Li, X.-J., and M. O. Marasteanu. 2010. "Using semi circular bending test to evaluate low temperature fracture resistance for asphalt concrete." *Exp. Mech.* 50 (7): 867–876. https://doi.org/10.1007/s11340-009-9303-0.

Linden, R. N., J. P. Mahoney, and N. C. Jackson. 1989. "Effect of compaction on asphalt concrete performance." *Transp. Res. Rec.* 1217 (1): 20–28.

Liu, Y., F. Gong, Z. You, and H. Wang. 2018. "Aggregate morphological characterization with 3D optical scanner versus X-ray computed tomography." *J. Mater. Civ. Eng.* 30 (1): 04017248. https://doi.org/10.1061/(ASCE)MT.1943-5533.0002091.

Liu, Y., X. Zhou, Z. You, S. Yao, F. Gong, and H. Wang. 2017. "Discrete element modeling of realistic particle shapes in stone-based mixtures through MATLAB-based imaging process." *Constr. Build. Mater.* 143 (Feb): 169–178. https://doi.org/10.1016/j.conbuildmat.2017.03.037.

Malvern, L. E. 1969. *Introduction to the mechanics of a continuous medium*. London: Pearson.

Man, T., J.-L. Le, M. O. Marasteanu, and K. M. Hill. 2022. "Two-scale discrete element modeling of gyratory compaction of hot mix asphalt." *J. Eng. Mech.* https://doi.org/10.1061/(ASCE)EM.1943-7889.0002033.

Masad, E., and J. Button. 2004. "Implications of experimental measurements and analyses of the internal structure of hot-mix asphalt." *Transp. Res. Rec.* 1891 (1): 212–220. https://doi.org/10.3141/1891-25.

Masad, E., V. K. Jandhyala, N. Dasgupta, N. Somadevan, and N. Shashidhar. 2002. "Characterization of air void distribution in asphalt mixes using X-ray computed tomography." *J. Mater. Civ. Eng.* 14 (2): 122–129. https://doi.org/10.1061/(ASCE)0899-1561(2002)14:2(122).

Masad, E., A. Scarpas, A. Alipour, K. R. Rajagopal, and C. Kasbergen. 2014a. "Finite element modelling of field compaction of hot mix asphalt. Part I: Theory." *Int. J. Pavement Eng.* 17 (1): 13–23. https://doi.org/10.1080/10298436.2013.863309.

Masad, E., A. Scarpas, K. R. Rajagopal, E. Kassem, S. Koneru, and C. Kasbergen. 2014b. "Finite element modelling of field compaction of hot mix asphalt. Part II: Applications." *Int. J. Pavement Eng.* 17 (1): 24–38. https://doi.org/10.1080/10298436.2013.863310.

McDaniel, R. S. 2019. *Impact of asphalt thickness on pavement quality*. Washington, DC: NCHRP Synthesis 537, Transportation Research Board.

Moutier, F. 1974. "La presse à cisaillement giratoire, modèle de série." In *Bulletin liaison ponts chausses*, 137–148. Paris: Institut Francais des Sciences et Technologies des Transports.

Peerlings, R. H. J., M. G. D. Geers, R. De Borst, and W. A. M. Brekelmans. 2001. "A critical comparison of nonlocal and gradient-enhanced softening continua." *Int. J. Solids Struct.* 38 (44–45): 7723–7746. https://doi.org/10.1016/S0020-7683(01)00087-7.

Peng, G., and T. Ohta. 1998. "Logarithmic density relaxation in compaction of granular materials." *Phys. Rev. E* 57 (1): 829. https://doi.org/10.1103/PhysRevE.57.829.

Risken, H. 1989. *The Fokker–Planck equation*. Berlin: Springer.

Rudnicki, J. W. 2015. *Fundamentals of continuum mechanics*. New York: Wiley.

Salamon, P., D. N. James, J. R. Harland, J. Pedersen, G. Ruppeiner, and L. Liao. 1988. "Simulated annealing with constant thermodynamic speed." *Comp. Phys. Commun.* 49 (3): 423–428. https://doi.org/10.1016/0010-4655(88)90003-3.

Stakston, A. D., H. U. Bahia, and J. J. Bushek. 2002. "Effect of fine aggregate angularity on compaction and shearing resistance of asphalt mixtures." *Transp. Res. Rec.* 1789 (2): 14–24. https://doi.org/10.3141/1789-02.

Tadmor, E., and R. E. Miller. 2011. *Modeling materials: Continuum, atomistic and multiscale techniques*. New York: Cambridge University Press.
Tashman, L., E. Masad, J. D'Angelo, J. Bukowski, and T. Harman. 2002. "X-ray tomography to characterize air void distribution in Superpave gyratory compacted specimens." *Int. J. Pavement Eng.* 3 (1): 19–28. https://doi.org/10.1080/10298430290029902a.
Tashman, L., E. Masad, B. Peterson, and H. Saleh. 2001. "Internal structure analysis of asphalt mixes to improve the simulation of Superpave gyratory compaction to field conditions (with discussion)." *J. Assoc. Asphalt Paving Technol.* 70 (1): 605–645.
Ter Huerne, H. L., M. F. A. M. Van Maarseveen, A. A. A. Molenaar, and M. F. C. Van De Ven. 2008. "Simulation of HMA compaction by using FEM." *Int. J. Pavement Eng.* 9 (3): 153–163. https://doi.org/10.1080/10298430701538091.
Thyagarajan, S., L. Tashman, E. Masad, and F. Bayomy. 2010. "The heterogeneity and mechanical response of hot mix asphalt laboratory specimens." *Int. J. Pavement Eng.* 11 (2): 107–121. https://doi.org/10.1080/10298430902730521.
Vavrik, W. R., and S. H. Carpenter. 1998. "Calculating air voids at specified number of gyrations in Superpave gyratory compactor." *Transp. Res. Rec.* 1630 (1): 117–125. https://doi.org/10.3141/1630-14.
Vavrik, W. R., W. J. Pine, and S. H. Carpenter. 2002. "Aggregate blending for asphalt mix design Bailey method." *Transp. Res. Rec.* 1789 (1): 146–153. https://doi.org/10.3141/1789-16.
Vivar, E. D. P., and J. E. Haddock. 2006. *HMA pavement performance and durability.* West Lafayette, IN: Purdue Univ.
Willoughby, K., and J. P. Mahoney. 2007. *An assessment of WSDOT's hot-mix asphalt quality control and assurance requirements*. Olympia, WA: Washington State Department of Transportation.
Yan, T., M. Marasteanu, C. Bennett, and J. Garrity. 2021a. "Field density investigation of asphalt mixtures in Minnesota." *Transp. Res. Rec.* 2021 (1): 03611981211009545. https://doi.org/10.1177/03611981211009545.
Yan, T., M. Marasteanu, and J.-L. Le. 2021b. "Mechanism-based evaluation of compactability of asphalt mixtures." *Road Mater. Pavement Des.* 22 (1): 482–497. https://doi.org/10.1080/14680629.2021.1905697.